Fermi National Accelerator Laboratory

FERMILAB-Pub-93/269

Characteristics of the Radiation Damage Seen in the Silicon Microstrip Detector of Fermilab Experiment E771

A. Boden et al

Fermi National Accelerator Laboratory
P.O. Box 500, Batavia, Illinois 60510

September 1993

Submitted to *Nuclear Instruments and Methods*

Operated by Universities Research Association Inc. under Contract No. DE-AC02-76CHO3000 with the United States Department of Energy

Disclaimer

Submitted to NIM August 27, 1993 FERMILAB-PUB-93/269
DUKE HEP-93/5

Characteristics of the Radiation Damage Seen in the Silicon Microstrip Detector of Fermilab Experiment E771

A. Boden[a], L. Fortney[c], V. Golovatyuk[f], W. Kowald[c], J. Lys[b], A. McManus[f], T. Murphy[d], W. Selove[e], R. P. Smith[d]

a. University of California at Los Angeles, Department of Physics, Los Angeles, CA 90024 USA

b. University of California at Berkeley, Department of Physics, Berkeley, CA 94720 USA

c. Duke University, Department of Physics, Durham, NC 27706 USA

d. Fermi National Accelerator Laboratory, Batavia, IL, 60506 USA

e. University of Pennsylvania, Philadelphia, PA 19104 USA

f. University of Virginia, Department of Physics, Charlottesville, VA 22901 USA

ABSTRACT

The central region of the silicon microstrip detector used in Fermilab experiment E771 was subjected to a peak fluence of 9.5 x 10^{13} p/cm^2 induced by 800 GeV protons over a two month period. Fourteen 300 μm thick planes manufactured by Micron Semiconductor were operated at bias voltages ranging from 84 to 109 V. Analysis of data from low intensity beam triggers taken near the end of the run shows that the mean pulse height from our amplifiers began to decline at a fluence of approximately 2 x 10^{13} p/cm^2 and fell to near zero by 6 x 10^{13} p/cm^2. We show that the use of fast amplifiers contributed to this early loss of signal.

1. Introduction

There have been several reported studies[1-7] on the deterioration of n-type silicon detectors after irradiation by high energy hadron beams with exposures of approximately 10^{14} p/cm^2. These beams produce significant displacement and transmutation damage in the silicon lattice, and have been shown[1] to convert wafers similar to ours from n-type silicon to p-type at a fluence of about 10^{13} p/cm^2. The bulk features of depletion depth and leakage current density are well understood, and studies[8] of the signal

shape from new and irradiated diodes[9] have also been reported, but there has apparently been no study of the signal from a fast amplifier responding to a fine pitch strip detector after irradiation has produced type-inversion.

As exposure levels rise above 10^{13} p/cm^2, it is known that higher bias voltages are needed to achieve full depletion of the silicon wafer, but there are apparent disagreements in the literature as to what constitutes an adequate bias for a 300 μm thick wafer at 20° C. Recent capacitance measurements[1, 7] of silicon wafers indicate that a bias voltage of 100 V will fully deplete our wafers up to about 4×10^{13} p/cm^2, but earlier studies[2, 4, 5] reported little loss of pulse height after exposures in excess of 10^{14} p/cm^2 with thickness scaled bias voltages in the range of 90-135 V.

The experience of the E771 experiment is that, in the area near the beam axis, our signal began to deteriorate very abruptly at about 2×10^{13} p/cm^2 to the point that the detector became essentially inoperative at 6×10^{13} p/cm^2. This suggests that our nominal 100 V bias was not sufficient to adequately deplete the wafers in the region of highest irradiation, but also indicates that some additional factor is needed to explain our early loss of signal amplitude.

In this paper we report on a study of the amplitude of the signal from our amplifiers in response to incident beam protons. The data used were taken in low intensity beam runs near the end of the experiment under otherwise normal running conditions. We show that the observed loss of signal amplitude after type inversion can be attributed to the use of fast amplifiers in conjunction with a fine pitch strip detector.

2. Running Conditions

Fermilab experiment E771[10] exposed eighteen new planes of a silicon microstrip detector (SMD) to a beam of 800 GeV protons. All planes of the SMD used n-type silicon wafers with p-type strips and were operated near a temperature of 20° C. There were six beam planes upstream of the target, the first four were manufactured by Hamamatsu on 250 μm thick wafers and had 250 μm pitch strips ; the other two beam planes and the twelve downstream planes were manufactured by Micron Semiconductor on 300 μm thick wafers. The Micron planes are 5 cm × 5 cm in transverse dimension

and were of two types: K and L. The K type planes have 384 25 μm wide strips on 50 μm pitch centers in the middle and 304 75 μm wide strips on 100 μm pitch centers on the outer edges . The L type planes were similar except with 15 μm strips on 25 μm pitch centers in the middle and 25 μm wide strips on 50 μm centers at the edges for the same number of strips but covering a smaller area. The beam was confined almost entirely to the 25 μm and 50 μm pitch sections of all planes. The arrangement, type, and numbering of the planes is shown in Fig. 1.

By the end of the run the Hamamatsu beam planes were being operated at bias voltages in the range 110-120 V, while the post-target Micron planes which are the focus of this study were at 84-109 V, several times the initial full depletion voltage of each plane and at or above the breakdown voltage rating given by the manufacturer.

Because only a small part of each strip was exposed to high fluence, leakage currents remained relatively low. At the end of the run we observed maximum strip leakage currents of less than 200 nA, well within the acceptable range for our preamps which were fast bipolar transimpedance amplifiers developed on an ASIC by the Research Division at Fermilab[11] These amplifiers featured an impulse response with a full width at half-maximum of about 15 ns, and were directly coupled to the strips, effectively grounding them through 200 Ω resistances.

We estimate that the total beam exposure was 5×10^{13} protons and that secondary particles produced in the target foils contributed an additional 36% to the total flux seen by the silicon wafers. Most of this exposure came during the last month of running when the beam intensity averaged 0.8×10^{9} protons/pulse. The integrated beam-plus-secondaries profile σ's in planes X4 and Y4 at the end of the run were 0.39 and 0.29 cm as determined by Gaussian fits to the corresponding leakage current profiles measured within a month of the conclusion of the run. With these profiles, we estimate a peak accumulated fluence downstream of the target of $9.5 \pm 3 \times 10^{13}$ p/cm^2 at beam center which was accumulating at the rate of 2.2×10^{12} p/cm^2 per delivered beam-day during the last month. The uncertainty in the value of the peak fluence is due to a number of uncertainties in determining the total integrated beam seen by the detector. In the following results this

uncertainty is displayed as a systematic error. We use the same fluence distribution for all planes downstream of the target, ignoring the dispersion of target secondaries and the accumulation of additional secondaries from interactions in the detector planes. None of the results described below has a significant correlation with plane position along the beam direction.

At several times during this experiment we collected data with low intensity beam triggers defined by a scintillator that was placed into the beam only for these runs. We previously reported[12] that 2D scatterplots of the intersections of X4,Y4,U1 hits in events from low intensity beam triggers taken near the end of the run showed an obvious lack of points near beam center. A similar plot made from events with unambiguous crossings of position-matched hits in the X1,X2 and in the Y1,Y2 Hamamatsu beam planes showed a similar result but exhibited the loss of hits in a smaller region around the beam center.

The voltage output pulse from our amplifiers was converted to a digital signal by a time-over-threshold post-amp-comparator which had a 10 mV hysteresis. The threshold of the comparator was set by a DAC output. The correspondence between DAC setting and the threshold voltage is shown in Fig. 2. In the region of interest the relationship is approximately linear at 0.29 mV per DAC count. On occasion we ran threshold studies using the low intensity beam triggers, varying the threshold from 40 to 90 DAC counts in ten count steps. Threshold settings during normal data acquisition at the end of the run were in the low 40's.

3. Data Analysis

Since the X1, X2, Y1, and Y2 beam planes are less affected[13] in the central region than the Micron planes, we are able to use these four planes to define beam tracks that can be used to determine the efficiency of each of the Micron planes as a function of x and y. Fig. 3 shows the efficiency of 1 mm squares of plane X4 determined in this way. This plot was made from low intensity beam triggers taken near the end of the run and is overlaid with contours of constant fluence as determined from the leakage current x and y profiles in planes X4 and Y4 as measured within a month after the run.

An estimate of the pulse height distribution is necessary to make the conversion from efficiency to mean pulse height. If the pulse height distribution is represented by a Gaussian g normalized to area one and T is the threshold, the efficiency E is given by

$$E(T,\bar{h},\sigma) = \int_T^\infty g(\bar{h},\sigma;h)\,dh \quad . \qquad 1$$

If σ and T are known, this equation can be inverted and solved for the mean pulse height $\bar{h}$ in terms of a measured efficiency.

A DAC threshold scan made early in the run was used to study the validity of the Gaussian assumption and to determine σ for the Gaussian representing the pulse height distribution. The run chosen shows very little evidence of radiation damage at the normal operating threshold, but the central dip in efficiency becomes quite clear at higher threshold settings. To make this study, we use beam tracks traversing the wafer through two narrow bands spanning the central region from -1 cm to +1 cm and containing the point of maximum fluence: one band is 4 mm wide and parallel to the x axis and the other is 5 mm wide and parallel to the y axis. The location of these bands on the wafer is shown in Fig. 3. Each band is transected into twenty equal rectangular areas so that there is little fluence variation across each area.

Using beam tracks defined by the Hamamatsu planes, we determine the efficiency of each rectangular area of each of the planes X4-X8 and Y4-Y8 at each of six threshold settings. For each area of each plane these efficiencies are plotted against DAC threshold as shown by the examples in Fig. 4 for six representative areas in the strip along the x-axis of plane X4. With the threshold T as the independent variable, efficiency Eq. 1 is fit to each of these plots, yielding an $\bar{h}$ and σ for each rectangle. These studies showed the pulse height distribution could be well represented by a Gaussian of essentially constant σ, independent of $\bar{h}$. A constant σ is qualitatively consistent with the expectations for electronic noise originating in the preamps and comparator. The error weighted average of σ was 23.7 for the X-planes and 23.3 for the Y-planes with r.m.s. variation of 1.2 and 1.0

respectively. In the following analysis we fix σ to one of these two values depending on the plane orientation.

The curves in Fig. 4 were determined by fixing σ at 23.7 DAC units and fitting Eq. 1 to determine the mean pulse height $\bar{h}$ in each rectangle. We cannot determine the integrated beam profile at this intermediate point in the run, but this figure shows that the fluence was already sufficient to produce a decrease in $\bar{h}$ near beam center.

Using the data from low intensity beam triggers taken at the end of the run, we next determine the efficiency of 1 mm^2 areas of each X and Y plane as in the X4 plane example shown in Fig. 3. Each of these efficiencies is then converted to a mean pulse height $\bar{h}$ using the appropriate average σ and threshold setting T. Fig. 5 shows the summarized results for each plane binned by fluence. Each mean pulse height on these plots is determined from the error weighted average of the $\bar{h}$ for areas lying within fluence contours like those shown in Fig. 3.

All planes show essentially the same behavior of a sharp break in the mean pulse height followed by an almost linear decline. The upturn in the measured pulse height at higher fluence on some of the planes (and in the center of Fig. 3) is believed to be an artifact caused by the low probability of detecting a true beam track in the highest fluence regions of the Hamamatsu planes.

The curve on each plot of Fig. 5 is from a three parameter fit of the mean pulse height p in terms of the fluence Φ using the function

$$\begin{aligned} &p = p_0 \text{ for } \Phi \le \Phi_c \\ &p = p_0\left(1 - \frac{\Phi - \Phi_c}{2(\Phi_h - \Phi_c)}\right) \text{ for } \Phi \ge \Phi_c, p > 0 \\ &p = 0 \text{ otherwise} \end{aligned} \tag{2}$$

where p_0 is the initial height, Φ_c is the fluence where the pulse height starts to decline, and Φ_h the fluence where it has declined to half of its initial value. There are significant plane to plane variations in both Φ_c andΦ_h, but their mean values are 2.1 and 4.3×10^{13} p/cm^2 respectively.

We have been able to reproduce the main characteristics of this mean pulse height behavior by combining the known radiation effects in silicon

with a calculation of the signal current collected on a strip of the detector. Initially, the bulk material in our silicon wafers was lightly doped to form a high resistance n-type semiconductor with heavily doped p-type implants forming the strips. After irradiation, the effective dopant density N_D can be described by the equation[7]

$$N_D = -N_0 e^{-c\Phi} + \beta\Phi \ , \tag{3}$$

in which N_0 is the initial density of n-type dopant, c describes the loss of this dopant, and β the generation of p-type dopants. The depletion voltage for a wafer is given by

$$V_D = \frac{q|N_D|w^2}{2\varepsilon} \ , \tag{4}$$

where q is the electron charge, w is the thickness of the detector, and ε the dielectric constant for silicon (1.054 pF/cm). Combining Eqs. 3 and 4 yields an expression for the change in depletion voltage with fluence.

$$V_D = \frac{qw^2}{2\varepsilon}\left|-N_0 e^{-c\Phi} + \beta\Phi\right| \ . \tag{5}$$

The parameter c has a typical value near 1.5×10^{-13} cm^2 and is important only at lower fluences. The more important quantity is β which has been variously reported in the literature[1, 2, 6, 7, 14] as having values between 0.018 and 0.05 cm^{-1}. The initial depletion voltages of our planes varied from 21 to 36 V, so our initial dopant density N_0 was about 4.0×10^{11} cm^{-3}.

For a typical detector, the type inversion described by Eq. 3 occurs at about 1×10^{13} p/cm^2, and above this fluence any undepleted zone begins to form from the p-side of the detector creating a field free layer of conducting material. But even in a fully depleted wafer with $V_{bias} > V_D$, type-inversion changes the gradient of the applied field E(z) as indicated in Figure 6a, lowering the field in the vicinity of the strips.

A minimum ionizing particle passing through the detector creates a thin line of hole-electron pairs that immediately begin to drift apart under the influence of the applied field. Neglecting diffusion, the drift velocity of a free charge in the bulk silicon is given by

$$\mathbf{v}_c(z) = \mu_c \mathbf{E}(z), \tag{6}$$

where μ_c is the mobility of the charge carriers. Electrons drift about three times faster than holes, and after type-inversion both charge carriers move slower near the collection strips where $\mathbf{E}(z)$ is smallest. This effect is most significant for the slower moving holes which drift toward the strips, slowing further and concentrating as they move into regions of lower field. Although the same amount of charge is ultimately collected from a strip, this change in drift velocity with increasing fluence broadens the current pulse and reduces its amplitude.

The weighting field method[15, 16] can be used to make a quantitative estimate of the current induced on the collection electrode. In this analysis, we are concerned only with beam tracks which are parallel to the z-axis. Simplifying further to consider only charge pairs produced along a line centered on the electrode, the electrode current is given by

$$i(t) = \left| \frac{q}{V_1} \mathbf{E}_w(z(t)) \bullet \mathbf{v}_c(z(t)) \right| \quad , \tag{7}$$

where the weighting field $\mathbf{E}_w$ is determined by fixing the collection electrode to voltage V_1 (typically 1 V) and grounding all others. For a diode of wafer thickness w, $|\mathbf{E}_w| = V_1/w$.

We have determined the weighting field[17] for 25 and 50 μm pitch strip detectors (15 and 25 μm strip widths respectively) from a numerical solution[18] of Laplace's equation on a 60 by 180 grid with 5 μm cells. All points on the boundary are set to zero potential except for the collection strip and the interval between it and the neighboring strips. In this between-strip interval the potential is assumed to fall linearly from unity to zero. Thus the nonzero portion of the 25 μm pitch detector is given by the sequence 0.333, 0.667, 1.0, 1.0, 1.0, 0.667, 0.333. The resulting weighting potential has a shape similar to that of the analytic solution for the more tractable boundary given in Ref. [19].

Along the electrode centered beam trajectory, we fit the numerical solution for the weighting potential to the form

$$V_w(z) = Az + \frac{B}{z-z_0} + \frac{C}{(z-z_0)^2} + \frac{D}{(z-z_0)^3} \tag{8}$$

with $D = D(A, B, C, z_0, w)$ defined so that $V_w(w) = 1$ V. Differentiation gives an expression for the magnitude of the weighting field

$$E_w(z) = a + b(z-z_0)^{-2} + c(z-z_0)^{-3} + d(z-z_0)^{-4} \tag{9}$$

with the coefficients for 25 and 50 μm pitches given in Table 1.

Table 1. Coefficients* of the weighting field

Pitch	a	b	c	d	z_0
25 μm	1.783×10^{-4}	-3.0579	1484.3	28.637	326.44
50 μm	3.9281×10^{-4}	-8.2226	4886.2	-2293.3	348.00

* All units are volts and μm.

In Figure 6b we compare these weighting fields with the constant field of a diode detector. Note that after type-inversion the weighting field for a strip detector is largest where the drift speed is smallest; drifting holes concentrate in this region producing a late peaking contribution to the current signal.

Eq. 6 describes the charge drift velocity as a function of $\mathbf{E}(z)$, but to avoid infinite drift times in regions of zero field we impose a minimum drift velocity of 1 μm/ns. The field $\mathbf{E}(z)$ can be described by the expression

$$|\mathbf{E}(z)| = \frac{V_{bias}}{d} - \frac{q}{\varepsilon} N_D\left(z - \frac{d}{2}\right) \quad , \tag{10}$$

where V_{bias} is the applied voltage, d is the thickness of depleted material, q is the electron charge, and ε the dielectric constant for silicon (1.054 pF/cm). In this expression $z = 0$ on the n-side. The concentration of dopant atoms N_D is a signed number which is initially negative and changes to positive with increasing fluence according to the Eq. 3. For this calculation[20] we have used c and β values of 1.1×10^{-13} cm^2, and 0.037 cm^{-1} respectively [7, 21] .

Using the 25 μm weighting field from Table 1, a bias of 100 V, and taking μ_c equal to 45 and 120 μm^{2}V^{-1}ns^{-1} for holes and electrons

respectively[15], we numerically determine the current derived from a line of charge pairs which at $t = 0$ are uniformly distributed along a beam trajectory in the undepleted thickness of the detector. Figure 7a shows a comparison of the charge collected on the electrodes of diode and strip detectors during 20 and 50 ns gates. Note that the 20 ns collection gate works fine for a diode or a new strip detector, but after type-inversion the charge collected from a strip starts to fall while V_{bias} is considerably greater than V_D.

In Fig. 7b, we show the result of convoluting electrode current signals with the impulse response of our 15 ns amplifier[11] and a hypothetical 30 ns version. The predicted signal for a strip detector is seen to be very similar to the experimental result presented in Fig. 5. Further, the model predicts that the signal will lose approximately half its initial amplitude when the fluence has increased to the point that $V_D = V_{bias}$. This result is not sensitive to changes in the constants c and β in Eq. 3 and changes only slightly for 50 μm pitch strips.

Fig. 8 shows the values of Φ_c and Φ_h determined from the fits of Eq. 2 to the data for each of the ten planes as shown in Fig. 5. The values are plotted against the bias voltage used on each plane. The simple mean and standard deviation of the difference $\Phi_h - \Phi_c$ for for all planes is $2.2 \pm 0.6 \times 10^{13}$ p/cm^2. The solid line in the figure is a one parameter fit of the expression

$$\Phi = \frac{2\varepsilon V_{bias}}{\beta q w^2} . \qquad (11)$$

to the Φ_h points under the model inspired assumption that the mean pulse height has fallen to half of its initial value whdn $V_D = V_{bias}$. This expression is the inverse of Eq. 5 with the small exponential term neglected. The fit yields $\beta = 0.033 \pm 0.011$ cm^{-1} where the quoted error comes from the systematic error on the total beam flux. There are significant variations between planes, and the two dashed lines show bounds that contain most of the planes: the limits are $\beta = 0.028$ and 0.040 cm^{-1}. Possible reasons for the variation between planes include cabling capacitance and timing.

4. Discussion

Although this determination of β is indirect and subject to a large systematic uncertainty, it is the first such measurement made after an exposure to a 800 GeV proton beam over a period of many weeks. The central value of β is larger than the values determined for 20° C wafers immediately after exposures of a few days. This may be partly due to higher levels of transmutational damage at our beam energy, but there may also be a connection with the annealing and anti-annealing processes[7] which occur with different time constants following few day exposures.

Since the most obvious way to increase the maximum fluence acceptable in the detector is to raise the bias voltage, we have run the model at 150 and 200 V biases. For a 25 μm pitch detector and the 15 ns current amplifier, the model indicates that in spite of generally shorter drift times, the signal continues to fall to about one-half of its initial value at the point where $V_D = V_{bias}$. However, the amplitude of the low fluence signal for these two voltages is larger than the 100 V value by 35 and 55% respectively.

We also note that the signal from a charge amplifier can be greatly improved by using a longer gate, but that the amplitude of the signal from a current amplifier is not similarly improved by doubling the width of its impulse response. This is a consequence of the late arrival of the drifting holes which have concentrated near the strip due to the drift speed gradient. The current from drifting electrons always peaks at $t = 0$, but after type-inversion the hole signal develops a double peaked character that lowers, broadens, and delays the output signal from a current amplifier. The delay is especially pronounced for 25 μm pitch strips.

5. Conclusions

We find that with a nominal 100 V bias, the output signal from our strip detector amplifiers began to decrease sharply at a fluence of about 2.5×10^{13} p/cm^2, and we have been able to understand this behavior in terms of recent measurements that quantify the rate of p-type dopant production combined with a detailed analysis of the signal generated by a single strip. Our analysis using the weighting field method indicates that with our amplifiers the output signal will fall to approximately half of its initial value

when $V_D = V_{bias}$, and that this model is consistent with our observations if the dopant production factor β is 0.033 cm^{-1}. The loss of signal while $V_D < V_{bias}$ is expected to be much less severe when the same amplifiers are connected to detectors with pad dimensions that are large compared to the wafer thickness.

Current amplifiers have the advantage of a fast recovery with no dead time, but it is apparent that they are also sensitive to the fluence dependent shape of the current signal from a strip detector. Increasing the bias voltage on the wafer reduces the drift time of charges (particularly the holes) at all fluences and can result in a larger signal from a current amplifier, but our model indicates that the signal will still be down by about 50% when $V_D = V_{bias}$.

Acknowledgments

We gratefully acknowledge the work of the members of the E771 collaboration who were involved in the mounting and running of this experiment, and thank the personnel of the Research and Computing Divisions at Fermilab for their contributions. We also thank T. Kondo, T. Ohsugi, and particularly Hans Ziock for many helpful discussions.

This work was supported by the U.S. Department of Energy and the National Science Foundation.

References

[1] E. Barberis, et al., Proceedings of the Sixth European Symposium on Semiconductor Detectors, Milan, Italy (1992)

[2] H. Dietl, et al., Nucl. Instum. Methods Phys. Res. A253 (1987) 460.

[3] J. S. Kapustinsky, et al., Proceedings of the International Conference on Adv. Techniques and Particle Physics, Como, Italy (1992)

[4] T. Kondo, et al., Proceedings of the 1984 Summer Study on Design and Utilization of SSC, Snowmass, Colorado (1984) 612.

[5] T. Ohsugi, et al., Nucl. Instum. Methods Phys. Res. A265 (1988) 105-111.

[6] H. J. Ziock, et al., IEEE Trans. on Nucl. Sci. 38 (1991)

[7] H. J. Ziock, et al., Proceedings of the IEEE Nuclear Science Symposium and Medical Imaging, Orlando, Florida (1992)

[8] H. W. Kraner, et al., Nucl. Instum. Methods Phys. Res. A326 (1993) 350.
[9] As used here, the term "diode" refers to any detector whose electrode dimensions are all comparable to or larger than the wafer thickness.
[10] B. Cox, et al. *Fermilab Proposal E771* (1986).
[11] D. Christian, et al., IEEE Trans. on Nucl. Sci. NS-36 (1988) 507.
[12] L. R. Fortney, et al., Proceedings of the DPF Meeting, Fermilab (1992)
[13] We now understand this superior performance after irradiation to be a consequence of the higher bias voltage and the use of significantly wider strips relative to wafer thickness.
[14] F. Lemeilleur, et al., IEEE NS 39 (1992) 551.
[15] E. Gatti and P. F. Manfredi, Riv. Nuovo Cimento 9 (1) (1986) 1
[16] V. Radeka, Ann. Rev. Nucl. Part. Sci. 38 (1988) 217-277
[17] This weighting field does not consider the effects of any conducting, undepleted layer near the p-strips so resulting amplifier output signals are not necessarily correct at fluences where the wafer is not fully depleted.
[18] W. H. Press, et al. in *Numerical Recipes*, 1st ed. (Cambridge University Press, Cambridge, 1986), 652–659.
[19] P. M. Morse and H. Feshbach. in *Methods of Theoretical Physics*, (McGraw-Hill, New York, 1953), 1175-1177.
[20] A different choice for the values for c and β is essentially a scale change of the fluence axis and does not affect the result that the mean pulse height falls to about half of its initial value when the depletion voltage equals the bias voltage.
[21] H. Ziock, Private Communication, May, 1993. This value of $\beta = 0.037$ is based on capacitance studies of large pad silicon detectors held at 0°C during few day exposures to 647 MeV/c protons, but is a better match to our six-week 800 GeV/c exposure than the 20°C measurement of $\beta = 0.018$.

Figures Captions

Fig. 1. Plane layout of the E771 silicon microstrip detector.

Fig. 2. Threshold voltage versus DAC setting.

Fig. 3. Efficiency of small areas of the central region of plane X4 at the end of the run overlaid with contours of constant fluence at intervals of 0.1 of the maximum fluence. Small negative efficiencies result from the correction for random hits.

Fig. 4. Each plot shows the efficiency versus DAC threshold in a small area of plane X4 at an early stage in the run. The fits are to a Gaussian pulse height distribution as described in the text. The mean pulse height corresponds to the inflection point of these curves.

Fig. 5. Pulse height as a function of fluence for the ten post-target X and Y planes. The fluence on each plot is units of 10^{13} p/cm^2. The fitted lines are described in the text.

Fig. 6. (a) The variation of the applied field across the thickness of the wafer as radiation damage increases from a to b. Note that after type-inversion the field strength is smallest near the strips located at z = 300 μm. (b) The "weighting field" for a diode and for single strips from our 25 and 50 μm pitch detectors. This field is evaluated along a beam trajectory centered on the strip and is determined by applying 1 V to the collection electrode and grounding all others.

Fig. 7. (a) The calculated fraction of the total charge collected in 20 ns and 50 ns gates as a function of fluence comparing a diode with a 25 μm pitch strip detector. (b) The relative amplitude of the output signal from our fast current amplifier and a slower one.

Fig. 8. Each solid marker shows the fluence Φ_h where the mean pulse height of a plane has fallen to 50% of its initial amplitude; the open markers show the fluence Φ_c defined by Eq. 2. Statistical errors are too small to display. The solid line is a one parameter straight line fit to the solid markers yielding $\beta = 0.033$, and the two dashed lines show $\beta = 0.028$ and $\beta = 0.040$ extremes. Square markers indicate *x*-planes, circles *y*-planes.

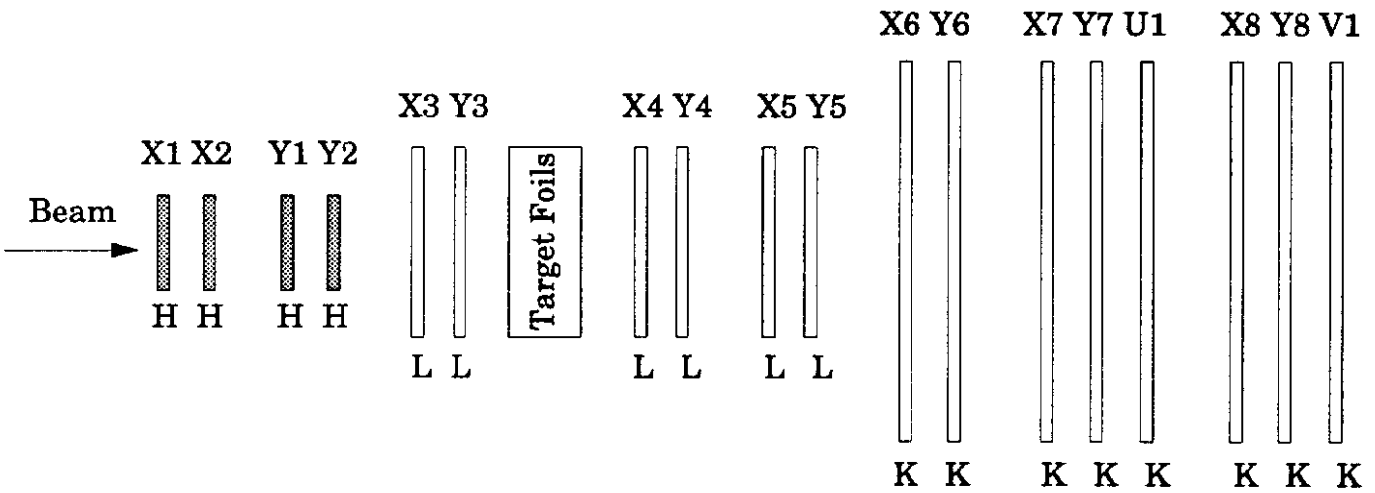

Not to scale

Figure 1

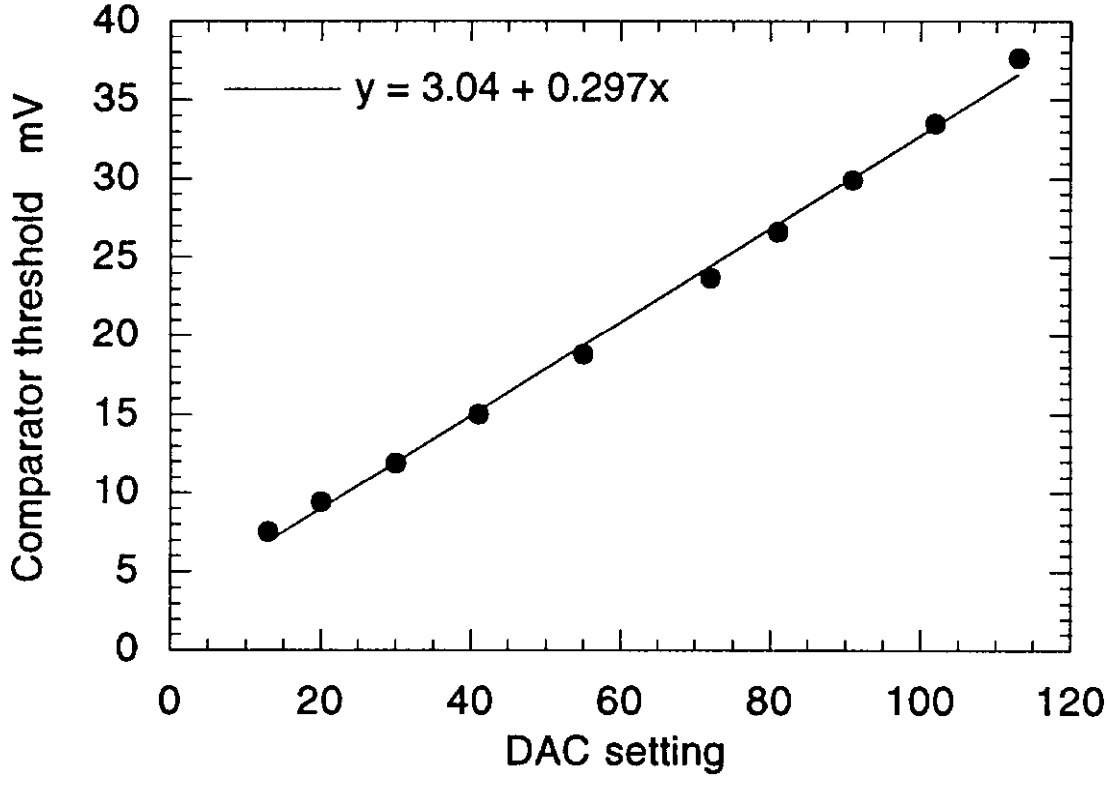
y = 3.04 + 0.297x
Comparator threshold mV
DAC setting
0
5
10
15
20
25
30
35
40
0
20
40
60
80
100
120

Figure 2

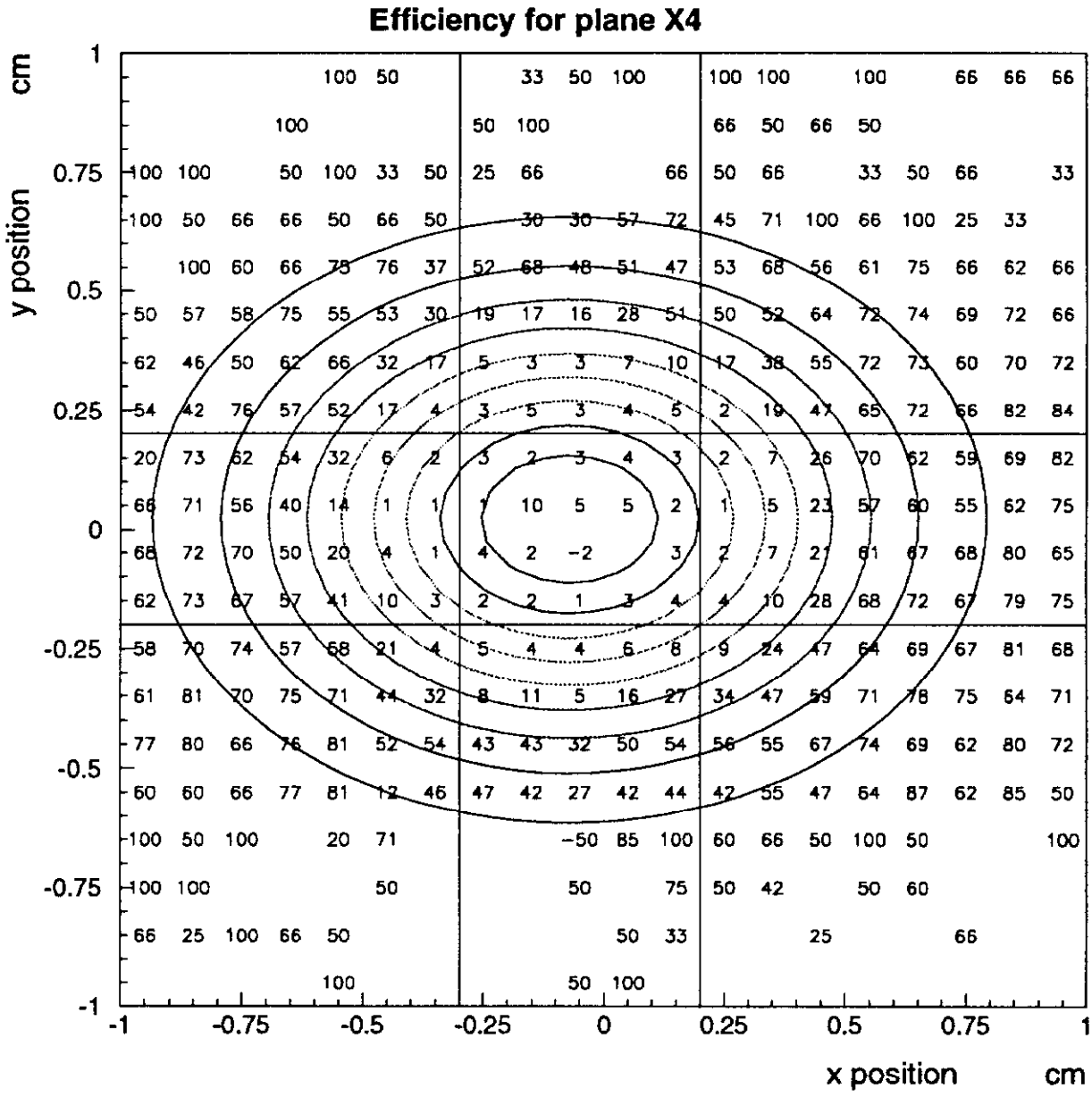
Efficiency for plane X4
y position
cm
x position
cm
1
0.75
0.5
0.25
0
-0.25
-0.5
-0.75
-1
-1
-0.75
-0.5
-0.25
0
0.25
0.5
0.75
1

Figure 3

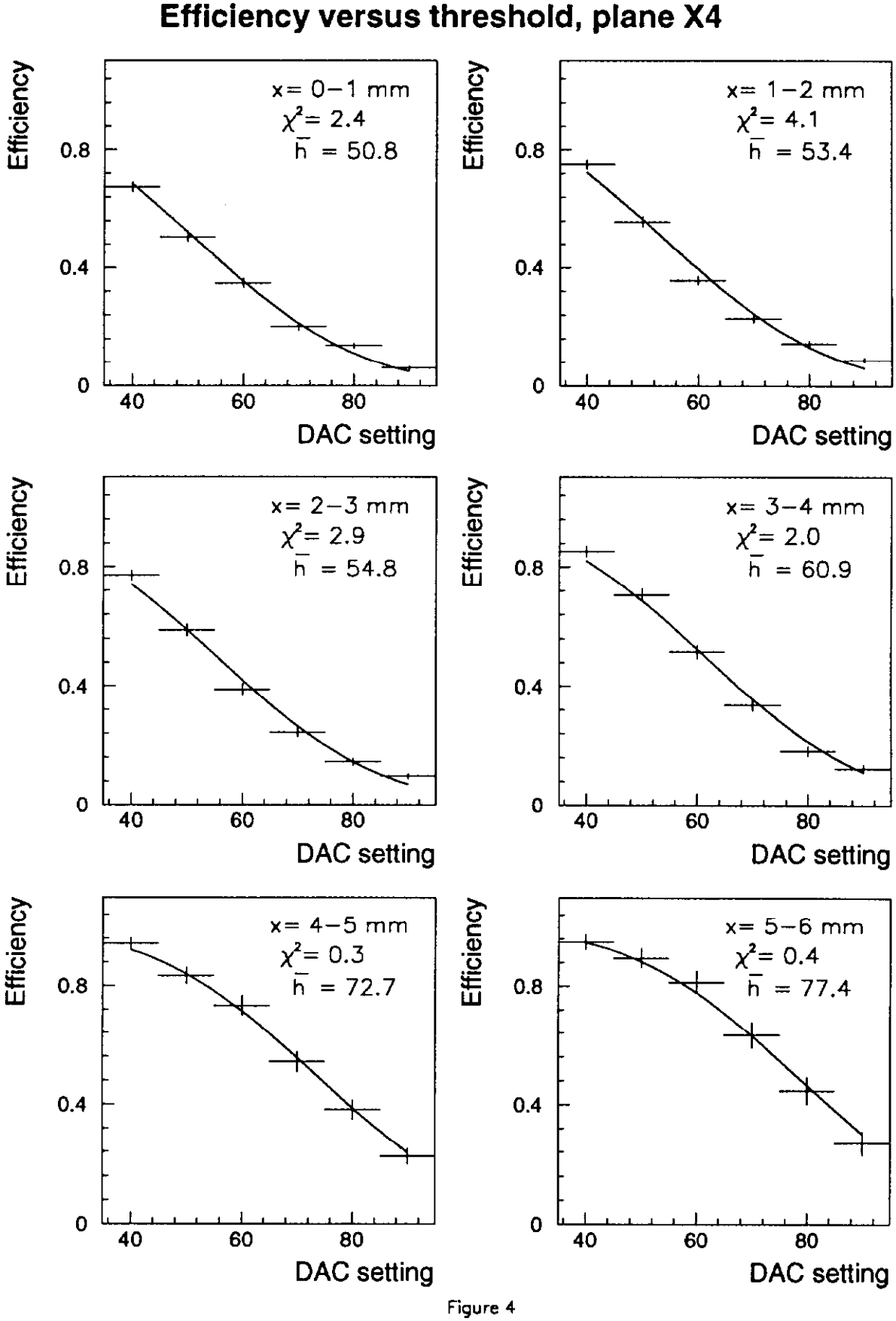
Efficiency versus threshold, plane X4
x= 0–1 mm
χ²= 2.4
h̄ = 50.8
x= 1–2 mm
χ²= 4.1
h̄ = 53.4
x= 2–3 mm
χ²= 2.9
h̄ = 54.8
x= 3–4 mm
χ²= 2.0
h̄ = 60.9
x= 4–5 mm
χ²= 0.3
h̄ = 72.7
x= 5–6 mm
χ²= 0.4
h̄ = 77.4
Efficiency
DAC setting
0
0.4
0.8
40
60
80

Figure 4

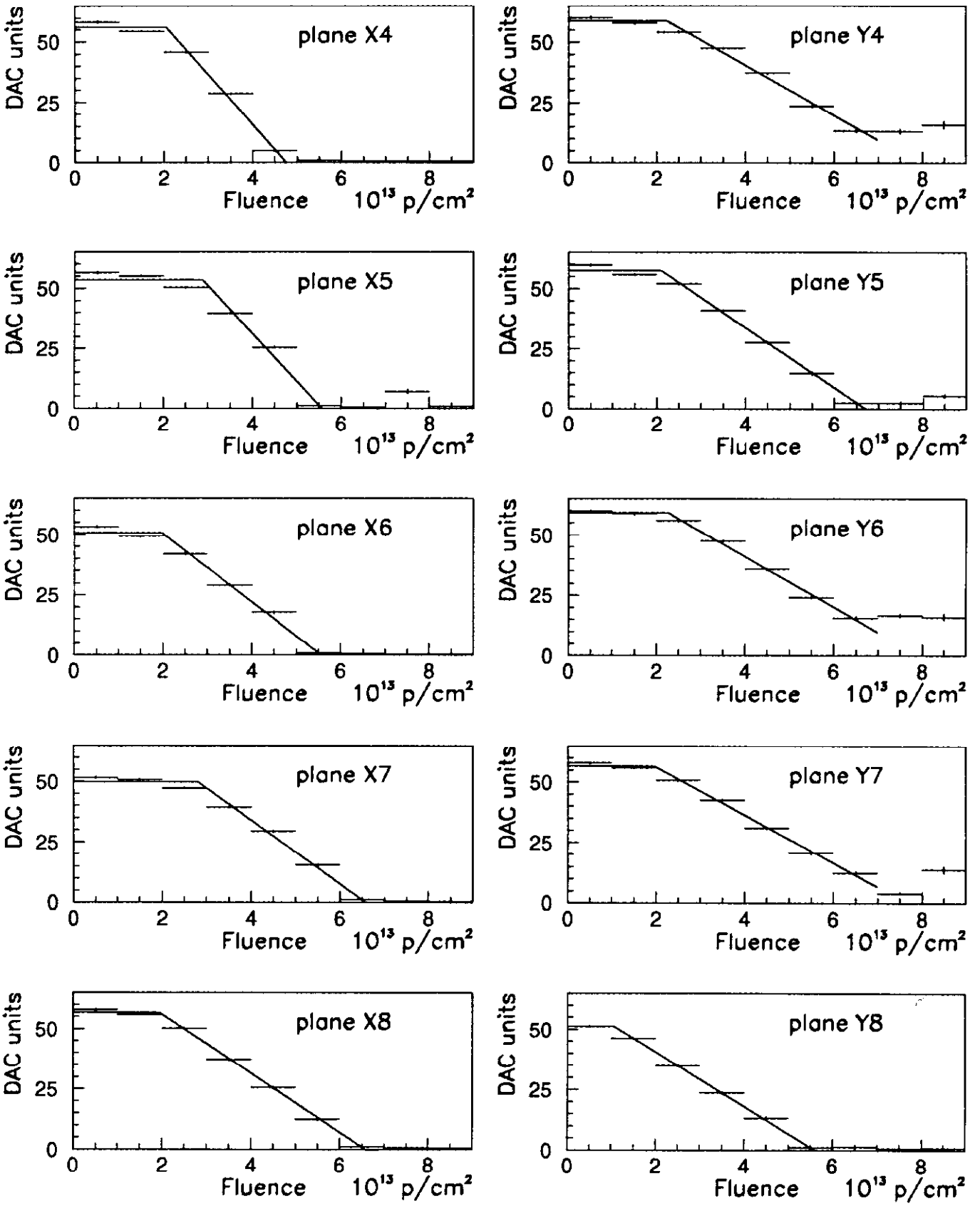
plane X4
plane Y4
plane X5
plane Y5
plane X6
plane Y6
plane X7
plane Y7
plane X8
plane Y8
DAC units
0
25
50
0
2
4
6
8
Fluence 10¹³ p/cm²

Figure 5

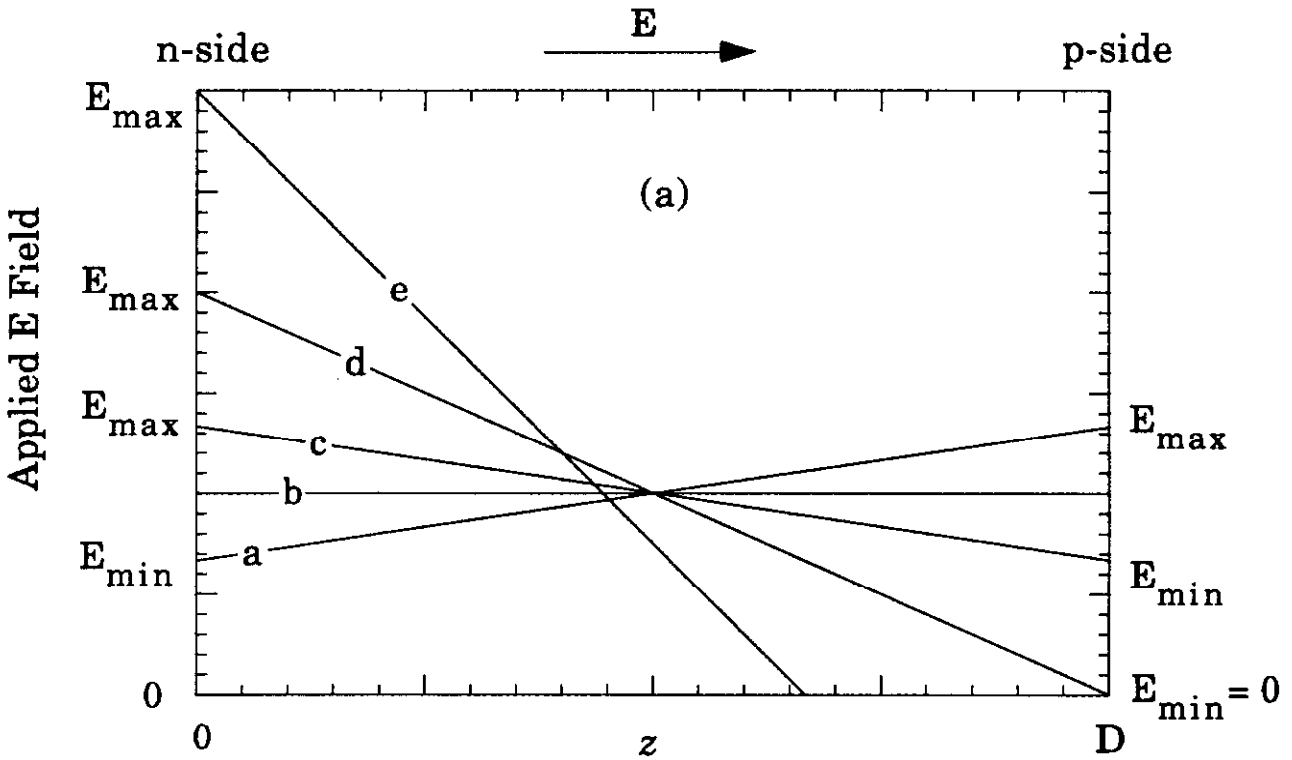
E
n-side
p-side
Applied E Field
E_{max}
E_{max}
E_{max}
E_{min}
0
(a)
e
d
c
b
a
E_{max}
E_{min}
E_{min} = 0
0
z
D

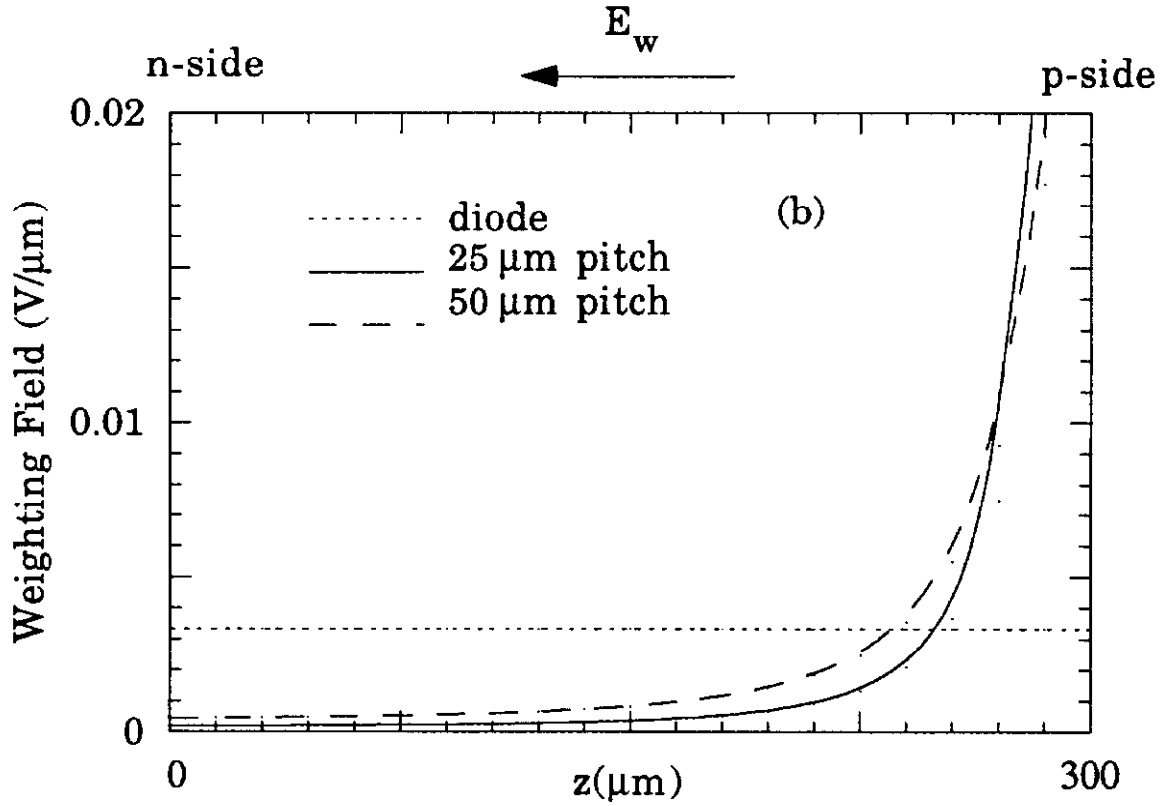
E_w
n-side
p-side
Weighting Field (V/μm)
0.02
0.01
0
(b)
diode
25 μm pitch
50 μm pitch
0
z(μm)
300

Figure 6

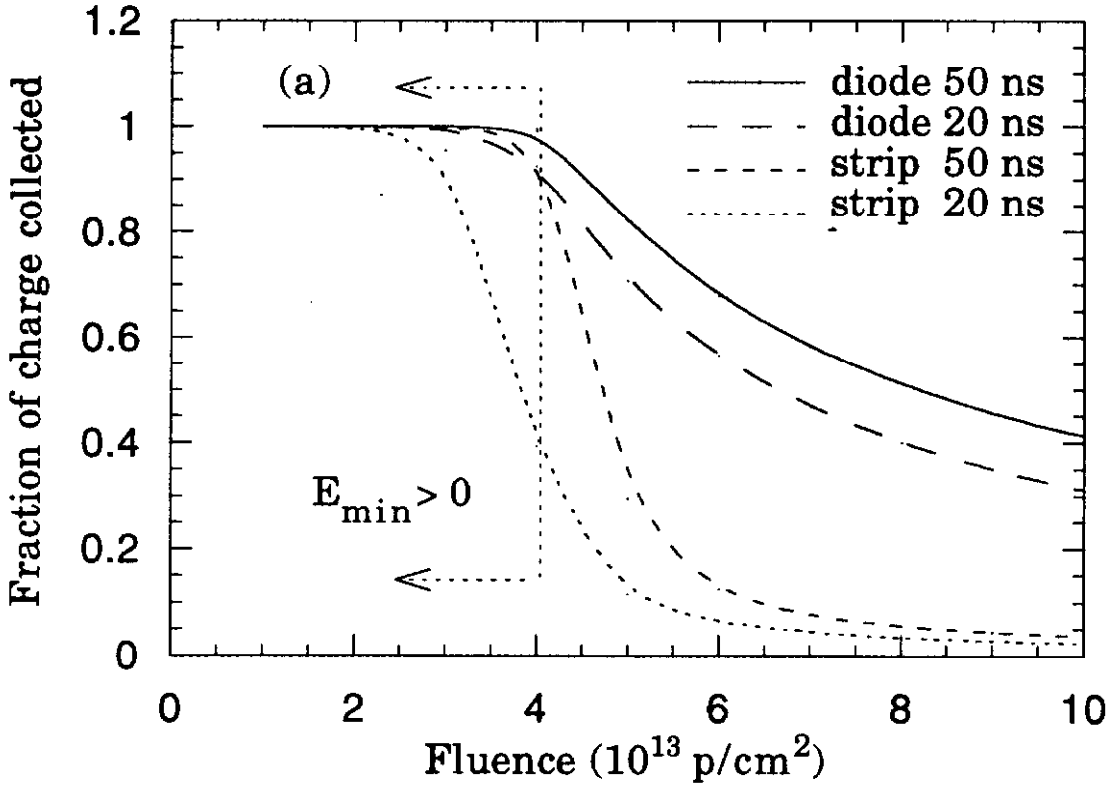
(a)
diode 50 ns
diode 20 ns
strip 50 ns
strip 20 ns
$E_{min} > 0$
Fraction of charge collected
Fluence (10^{13} p/cm^2)
0
0.2
0.4
0.6
0.8
1
1.2
0
2
4
6
8
10

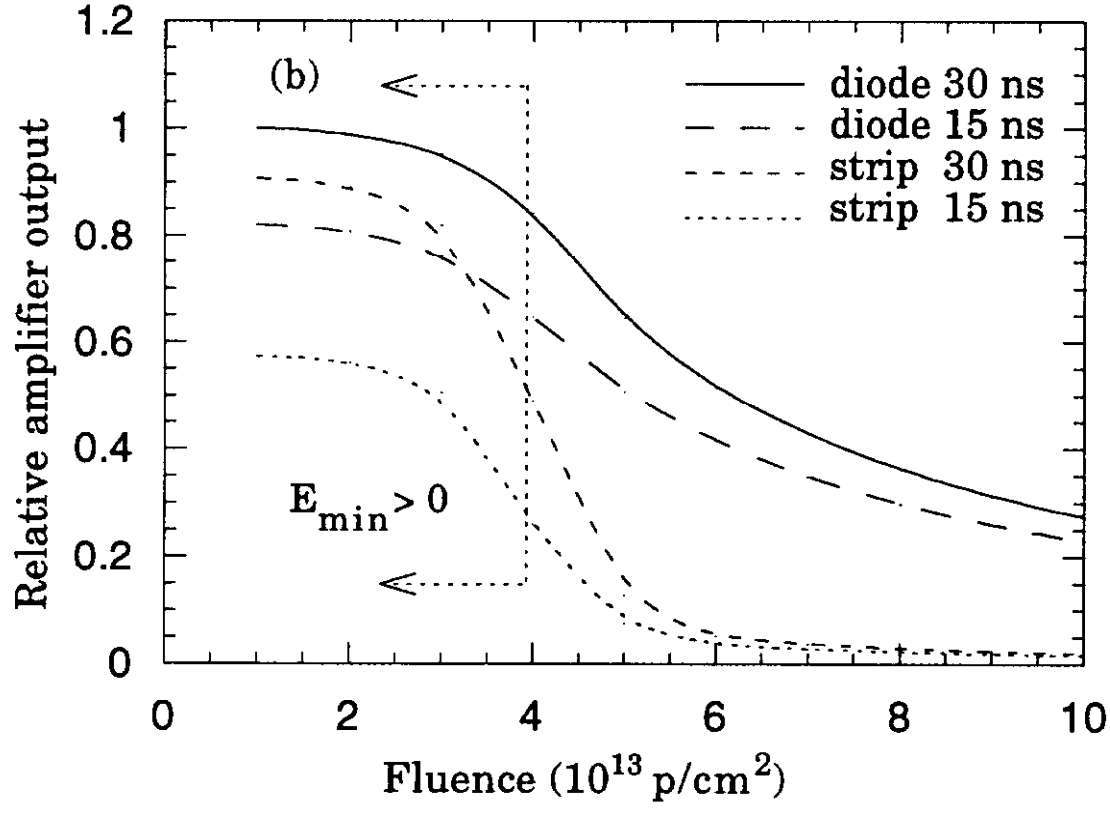
(b)
diode 30 ns
diode 15 ns
strip 30 ns
strip 15 ns
$E_{min} > 0$
Relative amplifier output
Fluence (10^{13} p/cm^2)
0
0.2
0.4
0.6
0.8
1
1.2
0
2
4
6
8
10

Figure 7

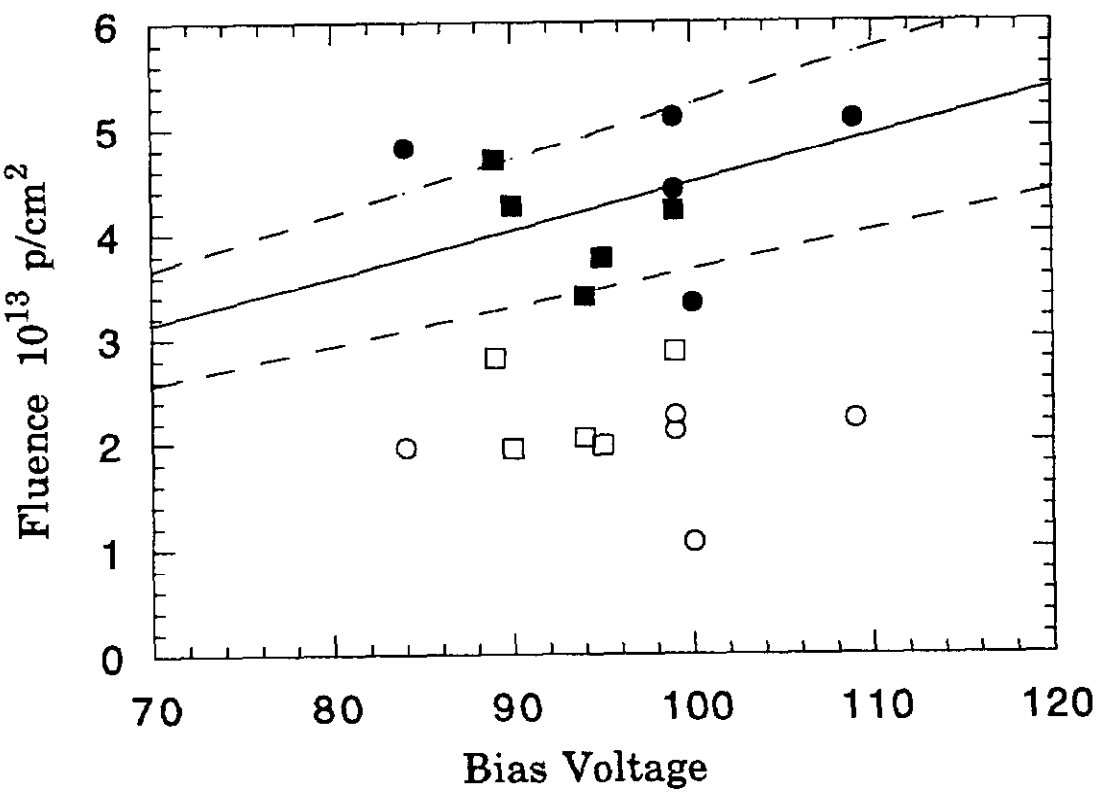

Figure 8